SC - R - 66 - 841

Sandia Corporation

REPRINT

CALIBRATION AND EVALUATION OF ACCELEROMETERS IN THE 10,000 g TO 100,000 g RANGE

by

R C Dove, R I Butler, and B W Duggin

OCTOBER 1965

DISCLAIMER

Issued by Sandia Corporation,
a prime contractor to the
United States Atomic Energy Commission

PREPRINT INSTRUMENT SOCIETY of AMERICA
20th Annual ISA Conference and Exhibit • October 4-7, 1965, Los Angeles
Preprint Number 17.3-1-65

CALIBRATION AND EVALUATION OF ACCELEROMETERS IN THE 10,000 g TO 100,000 g RANGE*

by

R. C. Dove, Head
Department of Mechanical Engineering
University of New Mexico
Albuquerque, New Mexico

B. W. Duggin, Staff Associate
Shock Test Division, 7325
Sandia Corporation
Albuquerque, New Mexico

R. I. Butler, Project Leader
Shock Test Division, 7325
Sandia Corporation
Albuquerque, New Mexico

Introduction

The ever-increasing severity of environments for which the test laboratories are required to instrument has resulted in a need for measuring accelerations at levels higher than that at which accelerometers can be evaluated by current calibration equipment. At Sandia Corporation, the interest in measuring the acceleration of vehicles subject to blast loading has resulted in a need to calibrate and evaluate accelerometers at levels up to 100,000 g. This paper describes a facility and techniques developed for evaluating accelerometers at this level.

Description of Facility

The requirements of such a facility are basically two: (1) a means of producing a suitable calibration pulse, and (2) a method of relating the voltage-time output traces to other measurements in order to interpret them as acceleration-time traces.

Pulses suitable for calibration purposes will be single clean pulses of the desired amplitude which are not accompanied by ringing and preferably not succeeded by oscillations. The pulse should not be narrow at the top since with such a pulse large changes in amplitude will result in only small changes in velocity (e.g., a half-sine shape is very good). It is not necessary for the amplitude of the pulse to be exactly predictable but it is necessary to be able to determine the maximum amplitude of the pulse. Furthermore, for calibration purposes, it is mandatory that we restrict ourselves to studying the amplitude sensitivity of the accelerometer (i.e., the voltage or charge output per g of acceleration amplitude) independent of frequency response and avoid pulses which will produce other than one-to-one seismic response. Therefore, to be useful for seismic accelerometer calibration, the calibration pulse must have a rise time of several times (say 2.5 or more) the natural period of the accelerometer and a total duration of many times (say five or more) the natural period. Typical natural periods of shock accelerometers that should be usable in the 10,000 g to 100,000 g range are between 8 μsec (125 kc) and 27.8 μsec (36 kc). This means that usable calibration pulses must have rise times in excess of 70 μsec ($\simeq$2.5 x 27.8) and total duration in excess of 140 μsec (>5 x 27.8). From this we can readily compute the velocity change that will be required. Assuming a triangular pulse:

$$\Delta V = \int a\,dt = 1/2\, A_{peak}\, t_{base}$$

$$= 1/2 \times \left(\frac{100,000}{1} \times 32.2\right)\left(140 \times 10^{-6}\right)$$

$$= 225 \text{ ft/sec.}$$

*This work was supported by the United States Atomic Energy Commission. Reproduction in whole or in part is permitted for any purpose of the U. S. Government.

Assuming a half-sine pulse:

$$\Delta V = \int a\,dt = 0.637\, A_{peak}\, t_{base}$$

$$= 0.637 \left(\frac{100{,}000}{1} \times 32.2\right) (140 \times 10^{-6})$$

$$= 285 \text{ ft/sec}$$

These velocities preclude the use of conventional pendulum or drop apparatus to produce the calibration pulse.

We have developed a small, variable-bore air gun which can be fired easily and repeatably, and which can drive a projectile at the required velocities. (See the Appendix for a description of this gun.) The acceleration pulses are shaped by momentum transfer between the projectile and an anvil upon which the accelerometer is mounted. A schematic of this setup is shown in Figure 1. This figure shows the air gun, the ram projectile in place, the accelerometer mounted upon an anvil, a mitigator for shaping the pulse, and the slotted portion of the barrel in which accelerometer and anvil are initially at rest. The barrel is slotted to permit bringing out the accelerometer cable, to permit triggering of the scope as the projectile passes a predetermined point, and to permit passing light beams which the accelerometer interrupts, thereby measuring the velocity of the accelerometer. We first attempted to produce the desired pulses by mounting the accelerometer on an aluminum piston and using steel and aluminum pistons as projectiles. Single clean pulses that were of a shape good for calibration were obtained. However, when we tried to go to levels above 60,000 g, the frequency associated with longitudinal wave vibration in the anvil-accelerometer combination became very predominant.*

Our next approach was to try the use of plastic projectiles with spherical section faces, theorizing that vibratory stresses induced in the projectile would not be transmitted across the interface between projectile and anvil due to the extreme acoustic impedance mismatch between the plastic projectile and the metal anvil. With

*It is interesting to note that this frequency cannot be predicted on the basis of longitudinal wave velocity in the anvil material and the length of the anvil. For example, with an aluminum anvil having a length of 1.25 inches the frequency associated with longitudinal wave propagation is computed as 80 kc.

$$f = \frac{1}{p} = \frac{\text{velocity propagation (in./sec)}}{2\ell\text{(in./cycle)}} = \frac{200{,}000}{2.5}$$

$$= 80 \text{ kc.}$$

However, when one type of accelerometer is mounted on this anvil the measured frequency is nearer 40 kc and when another (larger) accelerometer is mounted on this same anvil this frequency is reduced to 23 kc.

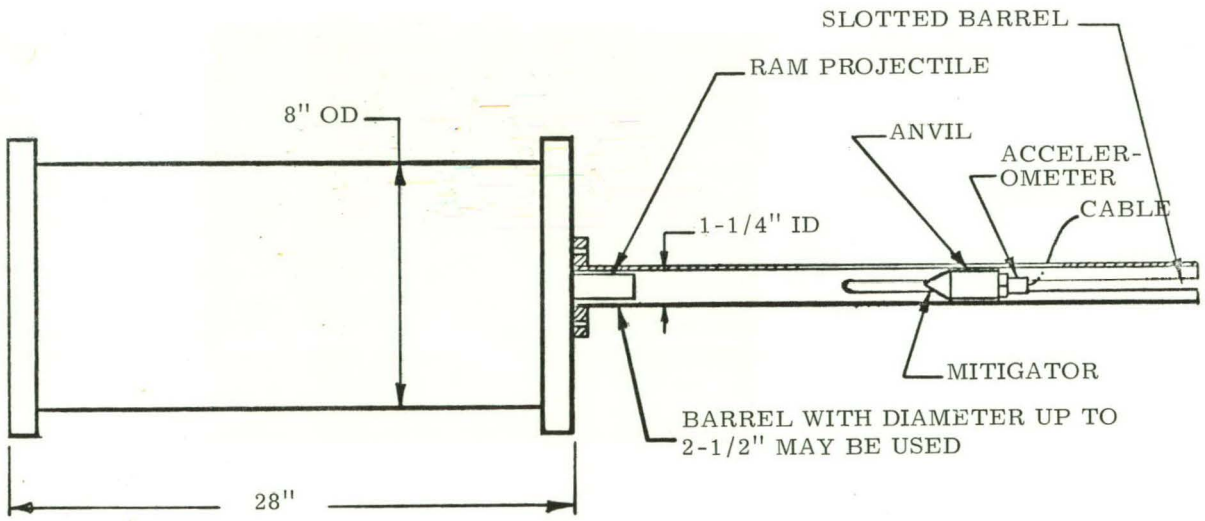

Figure 1 - Setup for accelerometer calibration using the small variable-bore air gun

this setup, however, we observed approximately the same limits on clean pulse amplitudes that were observed with the metal projectile and anvil. An analysis of the conditions indicated that the low acoustic impedance material, i.e., the plastic, would serve its function better as an anvil than as a projectile. Of the several setups investigated, the most suitable consisted of a metal projectile used to impact a nylon anvil through a mitigator of Ensolite* or a combination of Ensolite and felt. With this combination and the arrangement shown in Figure 2a, acceleration pulses in excess of 100,000 g having durations in excess of 100 μsec were easily obtained. However, the main pulse was followed by a series of oscillations which were felt to be undesirable if the calibration were to be accomplished by measuring changes in velocity. (See Figure 2b.) It was reasoned that if no tension could be developed across the joint between the anvil and the accelerometer, then no negative acceleration, and thus no oscillation, could occur. The stud connecting the accelerometer and the anvil was therefore replaced with a slip fit stud threaded only on the accelerometer end. The other end was slipped into a drilled hole in the anvil and, when a negative (tensile) load was demanded at the joint, the stud slipped in the hole and provided no negative loading. (See Figure 3a.) With this setup the acceleration pulse shown in Figure 3b was obtained. This pulse has a duration in excess of 100 μsec, has an indicated amplitude of about 100,000 g and is not followed by post pulse oscillations. Pulses of this type have been obtained repeatably with fairly predictable amplitudes.

*Ensolite is a flexible polyvinyl chloride foam manufactured by U.S. Rubber Company.

2a

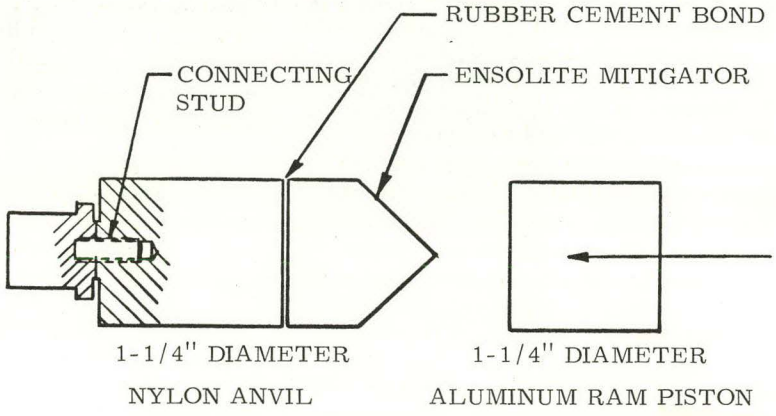

2b

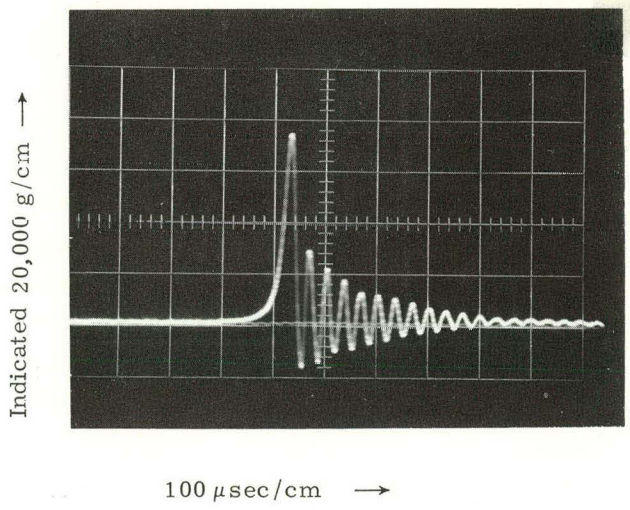

Figure 2 - Typical test setup and acceleration output trace with threaded stud

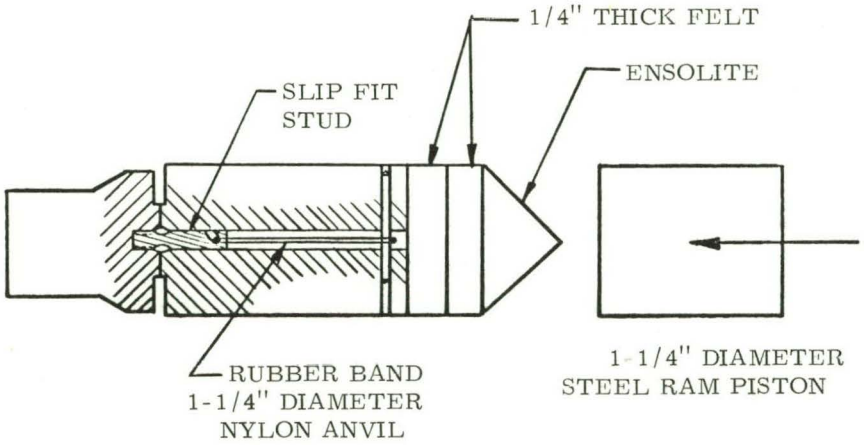

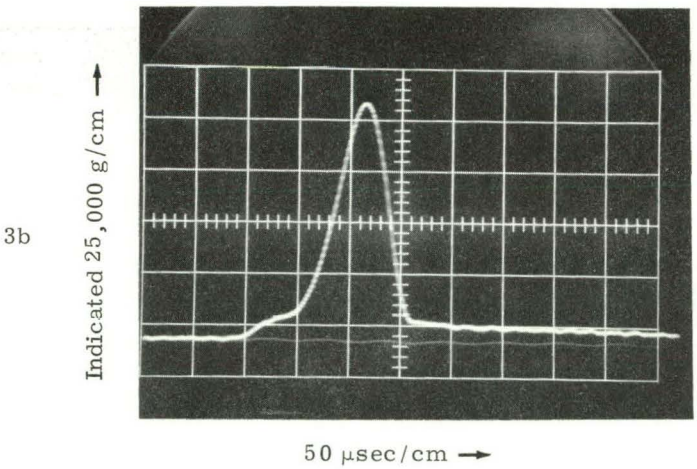

Figure 3 - Typical test setup and accelerometer output trace with slip fit stud

Reduction of Data

The production of an acceleration pulse of suitable amplitude, duration, and shape for calibration of accelerometers constitutes the first part of the calibration problem. The pulses shown, which have been called acceleration pulses, are of course only voltage-time pulses. It is necessary to interpret these pulses in relation to other measurements in order to convert the voltage amplitudes to acceleration amplitudes. The basic method used to accomplish this reduction consists of measuring the change in velocity of the accelerometer, and equating this measured velocity change to the area under the accelerometer signal-time curve. However, certain refinements in data analysis are incorporated which have not previously been applied.

The system used to measure velocity change is shown in Figure 4. The photodiode sensors are wired in a four-arm bridge as shown in Figure 5a, and a typical record obtained from this circuit is shown in Figure 5b. This system is calibrated by driving the anvil-accelerometer through the field with a depth micrometer. This is essentially a static calibration, but it has been checked against a 35-gigacycle-per-second* microwave interferometer over the entire velocity range in which it has been used.

Since the accelerometer is initially at rest, the velocity change is equal to the velocity after the acceleration pulse. This is obtained by dividing

*One gigacycle = 10^9 cycles.

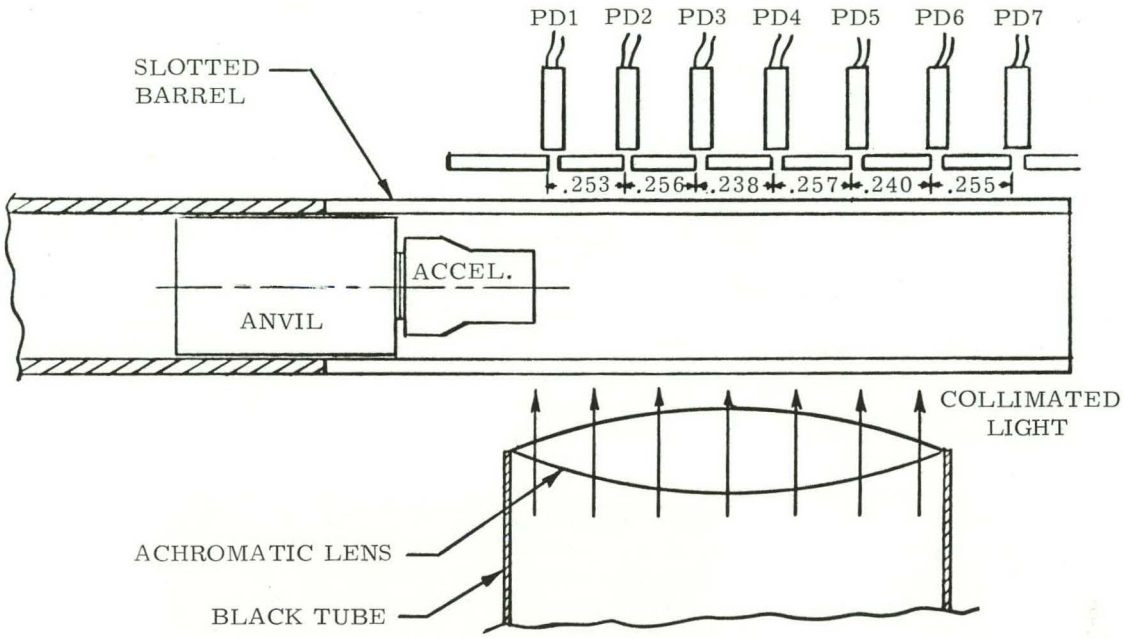

Figure 4 - Setup for velocity measurement

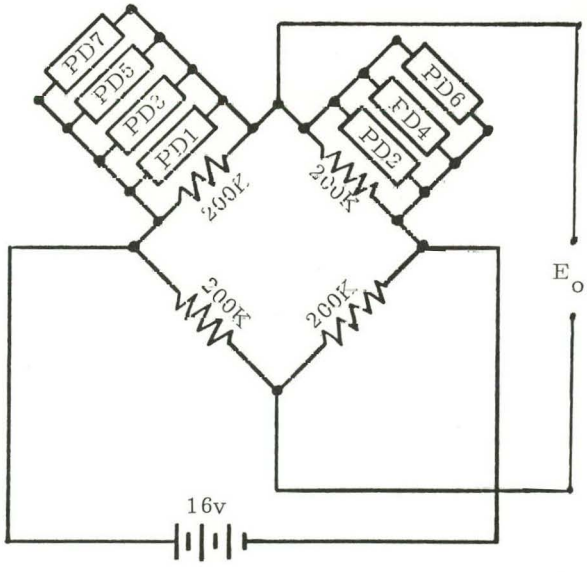

Figure 5a - Circuit for measuring output of photodiodes illustrated in Figure 4

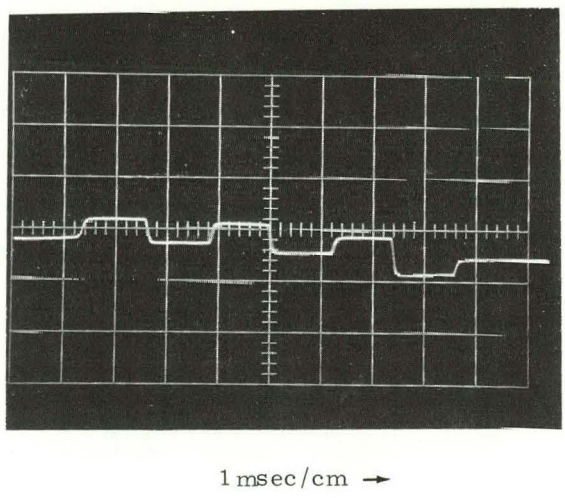

Figure 5b - Output trace of photodiode circuit of Figure 5a

the distance between any two diodes by the time of passage between these two points. By using a series of diodes instead of only two it is possible to determine a decrease in velocity after the acceleration pulse due to any cause.

When one measures the velocity following a pulse and utilizes this measurement to determine the sensitivity of an accelerometer, he is required to make certain assumptions. Figure 6 illustrates the computation generally made. The output of the accelerometer being in volts, the area under the accelerometer trace has the units volt-seconds. The velocity, measured by other means such as by photodiodes a fixed distance apart, can be stated in g-seconds. The ratio of area to the velocity change then provides the sensitivity of the accelerometer as (x/y) volts/g. For convenience this value is usually given in mv/g. Ordinarily this procedure is repeated for several different values of maximum acceleration and the values of accelerometer sensitivity versus peak indicated g are plotted. If the ratio (x/y) (i.e., the accelerometer sensitivity) were to remain unchanged, the curve labeled (1) in Figure 7a would be obtained and the accelerometer output would be a linear function of acceleration amplitude within the range checked. For such an accelerometer, the plot of voltage output against acceleration input is a straight line; as indicated by curve (1) in Figure 7b. For this condition, the procedure outlined above is completely adequate for accelerometer calibration. If, however, the output of the accelerometer increases faster than the acceleration input [as suggested by curves (2) and (3) on Figure 7b], certain refinements must be made in order to calibrate an accelerometer using the above procedure. If, for example, the accelerometer sensitivity increases linearly with acceleration level, as shown by curve (2) in Figure 7a, then the relationship between accelerometer voltage output and acceleration is as shown in Figure 8a. In this idealized trace the maximum acceleration amplitude has been taken arbitrarily as that value where the accelerometer sensitivity has increased linearly to 20 percent above the zero level sensitivity. The maximum acceleration amplitude has been normalized to unity and the maximum amplitude of the actual voltage output trace has been normalized to unity times the increase in accelerometer sensitivity (i.e., 1.2 at maximum amplitude). Then at midheight the acceleration amplitude is 0.5 and the amplification of signal is one-half the maximum amplification or 1.1. Therefore, the normalized midheight voltage output is 0.5 x (1.1) or 0.55. If the area under the acceleration-time trace is also normalized to unity, integration of the voltage-time trace will produce an area equal to 1.156.

However, when the accelerometer sensitivity is established by equating the area under the voltage-time curve to the change in velocity, it is tacitly assumed that the relationship between accelerometer voltage output and acceleration is as shown in Figure 8b -- i.e., it is assumed that sensitivity is constant over the entire acceleration range covered in this shock. For the conditions assumed in this example, if the area

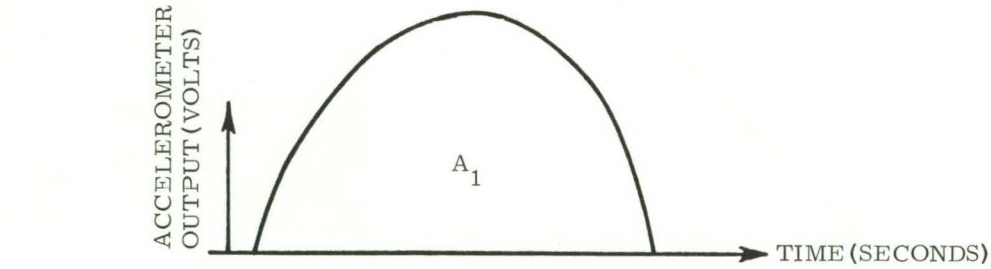

Figure 6 - Determination of accelerometer sensitivity by comparing area under acceleration-time trace to the measured velocity

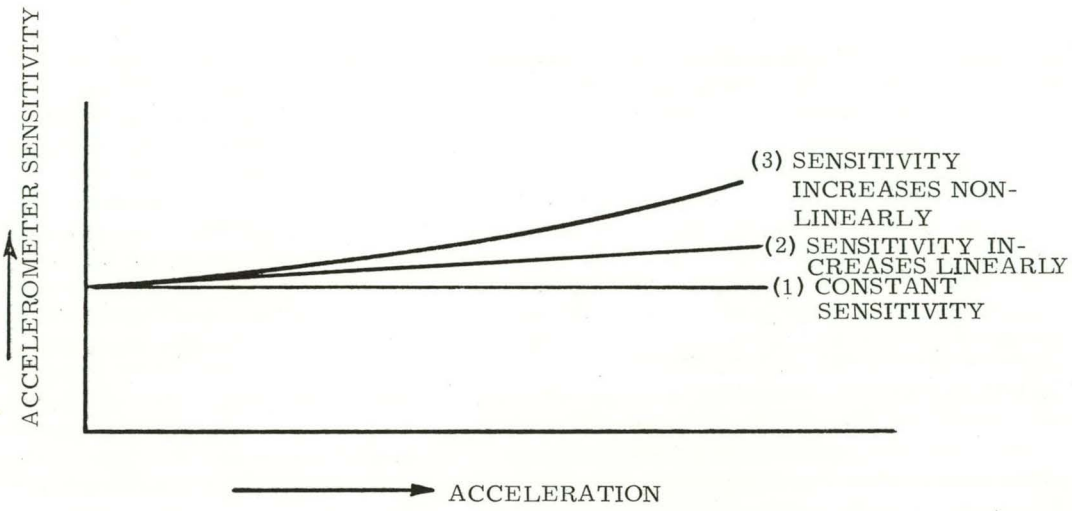

Figure 7a - Plot of accelerometer sensitivity versus acceleration input level

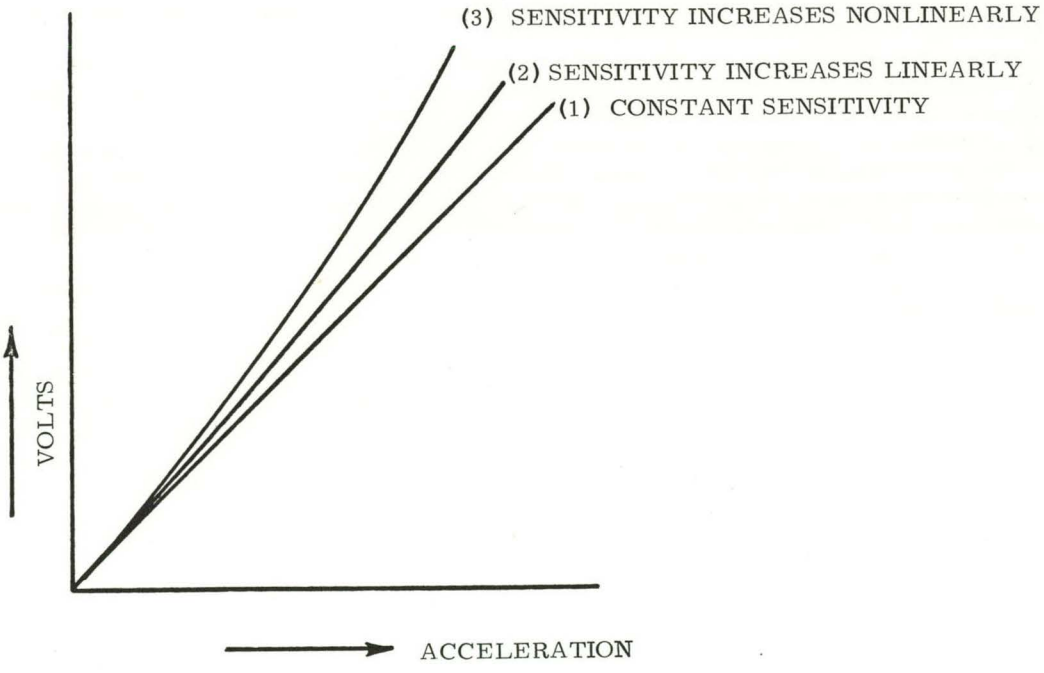

Figure 7b - Plot of accelerometer output (volts) versus acceleration input level

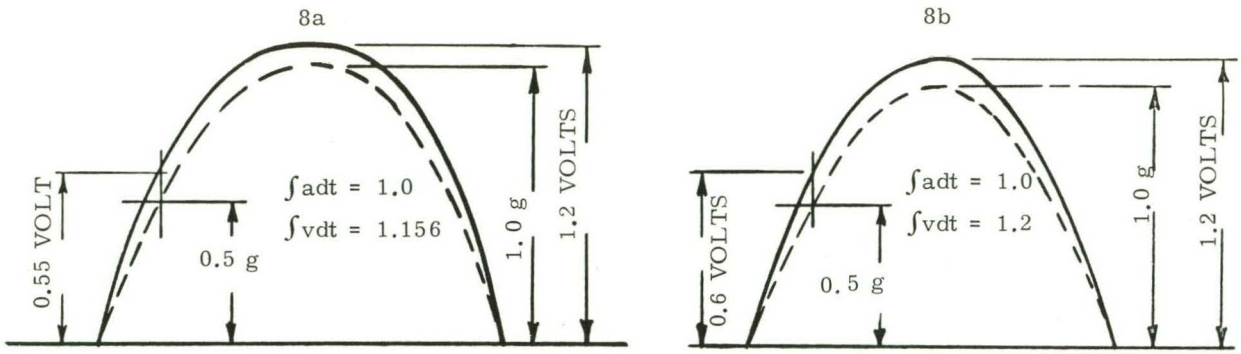

NOTE: — — — Actual Acceleration Trace (g)
——— Accelerometer Output (volts)

The acceleration amplitude has been normalized to unity, and the zero level accelerometer sensitivity normalized to 1.0 volt/g. The area under the actual acceleration-time trace has been normalized to unity.

Figure 8a - Output of accelerometer with sensitivity varying linearly with input. Maximum amplitude arbitrarily taken at the 20 percent nonlinear point.

Figure 8b - Assumed shape of the accelerometer output trace when using the method of Figure 6 to determine accelerometer sensitivity.

under the acceleration-time trace is normalized to unity, the area under the assumed voltage-time trace is merely equal to 1.2 since all voltage ordinates have been increased by 20 percent. The difference between the areas of the actual and assumed accelerometer output curves then represents the error in using the method of Figure 6 to determine accelerometer sensitivity--i.e., for a half-sine pulse of sufficient amplitude to produce an increase of 20 percent in the accelerometer sensitivity and for those accelerometers for which the sensitivity changes linearly with acceleration input, the error in determining accelerometer sensitivity by the method of Figure 6 for the level shown is approximately 4 percent.

Of course, this error will be different for various acceleration-time pulse shapes. In general, the error will be greater as the centroid of the area of the acceleration-time pulse is lowered relatively to the pulse peak. That is, the error is greater for pulses characterized by narrow peaks superposed on a broader base--the type most commonly encountered. Further, if the sensitivity versus acceleration curve is as suggested by curve (3) in Figure 7b (i.e., the sensitivity varies nonlinearly with acceleration level), then the error in this form of analysis will again be increased.

In the present work it was anticipated that the accelerometer sensitivity would vary with the acceleration level; therefore, the data was reduced as follows. The accelerometer signal-time record was integrated using the accelerometer sensitivity established at a near zero g level (shake-table test). The ratio of velocity change so computed to measured velocity change was plotted versus indicated peak acceleration. Some idealized data are shown in this form as Figure 9. Study of such a plot gives a first approximation as to the way in which sensitivity varies with acceleration. Brief theoretical analysis shows that, for versed sine pulses, the ratio of ΔV (by integration) to ΔV (measured) would be 1.19 if the sensitivity increased linearly to 125 percent of its "zero" g value at 100,000 g. Therefore, for the data plotted as Figure 9 we would "guess" that this accelerometer shows a linear increase in sensitivity (N) of 25 percent in 100,000 g. All ordinate values on the accelerometer signal-time trace are now corrected accordingly and the resulting "corrected" acceleration-time curve is re-integrated. If the assumed correction is the correct one, this same correction will apply to the data obtained from a series of tests covering a wide range of peak acceleration levels. As a result, when ΔV by integration of corrected data versus ΔV measured is plotted against corrected acceleration values, the result will be a horizontal line as shown by curve (1) in Figure 10. If (N) had been assumed too high or too low, [curves (2) and (4) respectively in Figure 10], or if the increase were actually nonlinear [curve (3) in Figure 10], the above computations would be repeated with new assumed values of (N) or

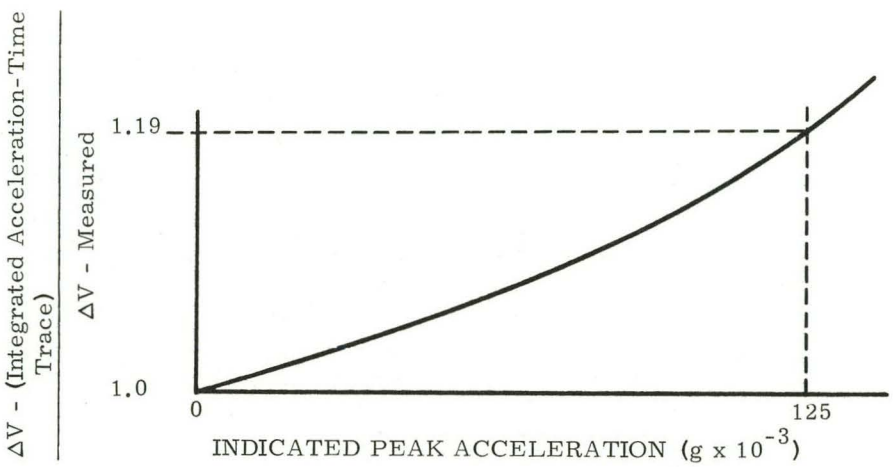

Figure 9 - Idealized plot of ratio of integrated-to-measured velocity change versus acceleration input level

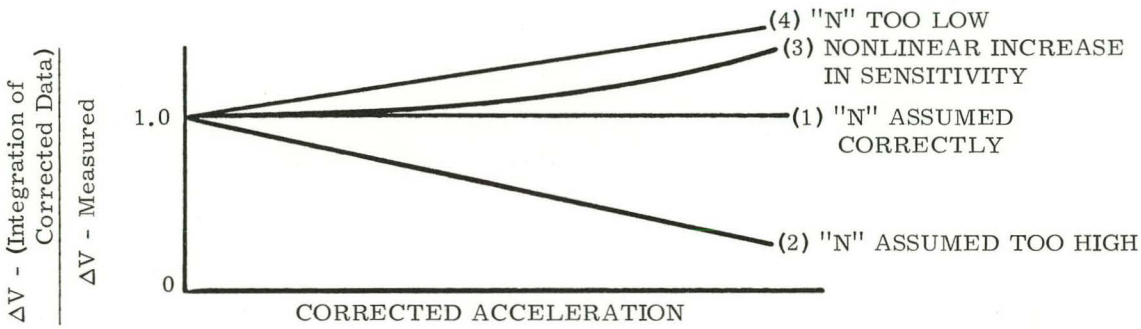

Figure 10 - Plots of corrected data of Figure 9 based on various assumptions of accelerometer sensitivity variation

with nonlinear correction factors until curve (1) in Figure 10 was obtained.

Force Measurement

Force monitoring has also been used in data analysis to supplement the information obtained from measured velocity change. However, because of the need to maintain a system with as high a natural frequency as possible, it has not been possible to use conventional load cells on which the accelerometer, or the accelerometer together with an anvil, could be mounted. Instead, in some tests the accelerometer has been mounted directly on a disk of x-cut quartz as shown in Figure 11. The electroded surfaces are bonded to silver foil washers with Eastman 910 cement, the silver foil washer at the accelerometer interface is in turn bonded, with Eastman 910 cement, to the accelerometer base. The silver foil washer at the anvil interface is not bonded to the anvil. The electrode at the accelerometer interface is electrically connected to the shield of a coaxial cable and is common with the case of the accelerometer (ground); the electrode at the anvil interface is connected to the center wire of a coaxial cable.

This crystal functions to measure the force applied to the base of the accelerometer and hence it can be directly related to the accelerometer signal through the accelerometer mass. With our present setup, however, factors such as the variations in the way the quartz disk is loaded from test to test and uncertainty of the effective accelerated mass have precluded the use of the quartz disk as an actual calibration

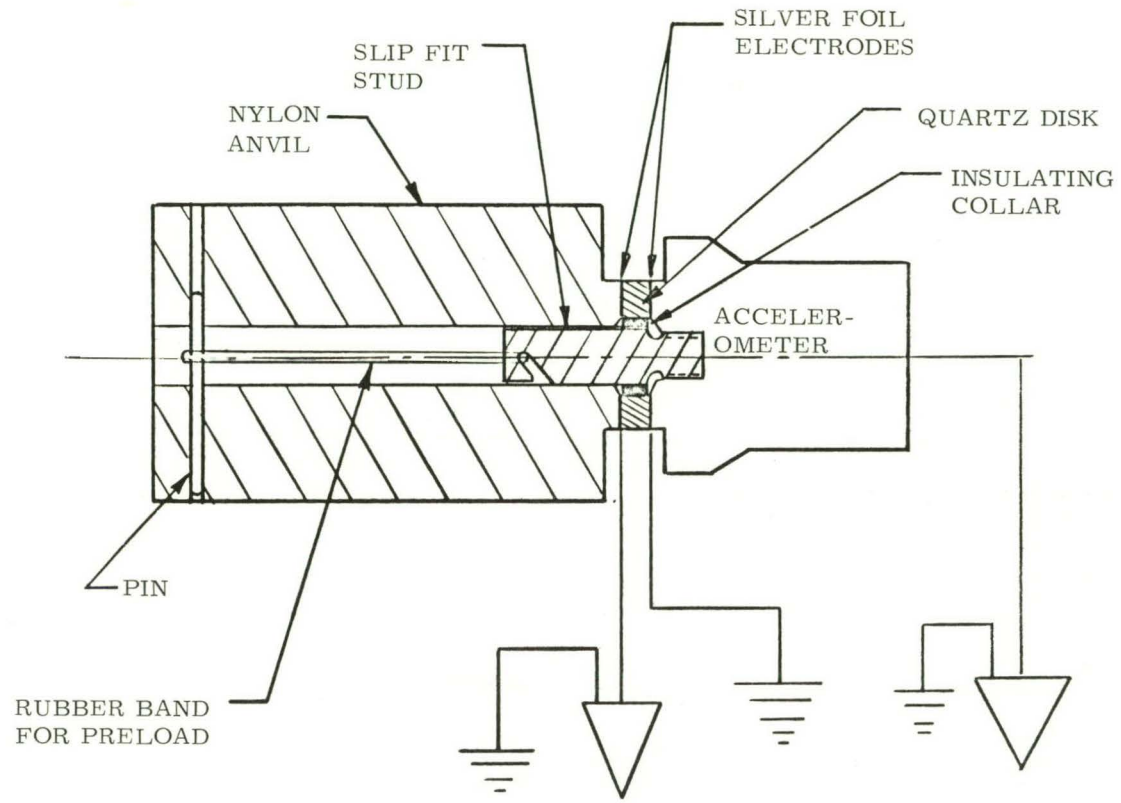

Figure 11 - Quartz disk load cell used to measure force applied to base of accelerometer

standard. With refinements in the setup and changes designed for precise force measurements, it is anticipated that kinetic calibration can be utilized in the near future.

The output of this force transducer has been most useful in separating true acceleration signal from accelerometer zero shift. Note that in Figure 12 the accelerometer produces a positive output after the force applied to the base of the accelerometer (as measured by the quartz crystal) has gone to zero. Until the addition of the quartz disk, computation of the area under the acceleration-time trace was complicated when zero shift was present by the uncertainty of the end of the pulse.

We have found that the presence of the quartz crystal does not affect the pulse shape.

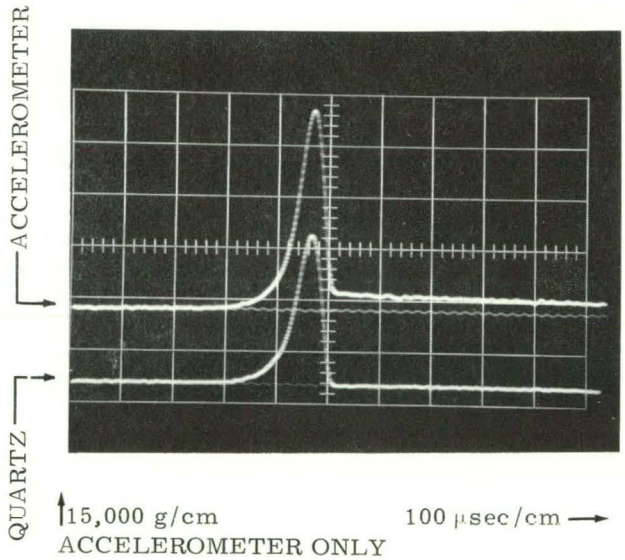

Figure 12 - Oscilloscope traces of accelerometer and quartz disk outputs

Results

Data obtained from a series of tests on one experimental accelerometer are presented in Figures 13 and 14 as an example of the use to which this facility has been put. In Figure 13 the ratio of velocity change obtained by integrating the accelerometer signal-time trace to the measured velocity change is plotted versus the indicated value of peak acceleration. From this plot it is clear that the sensitivity of this accelerometer is increasing with increasing acceleration level. Therefore, we guess that the sensitivity of this accelerometer increases linearly with acceleration level such that its sensitivity has increased by 100 percent at 100,000 g true acceleration level.* Figure 14 shows the same original data replotted after the accelerometer data has been modified on the basis of the assumed linear increase in sensitivity. Because this modification results in a constant value of the ratio of integrated accelerometer signal-time trace to measured velocity change, we conclude that the assumption is correct.

The following characteristics of this experimental accelerometer are also of interest. Above 10,000 g this accelerometer shows positive zero shift when subjected to unidirectional pulses (see Figure 12). Use of this accelerometer to measure pulses in excess of 60,000 g does not change the low-level sensitivity, however. During this study the accelerometer was recalibrated at the 1000-g level after every two or three tests at higher g levels and no change in sensitivity was found.

It is our intention to use this facility and the data reduction techniques discussed to evaluate various accelerometers now in use, to establish (1) their general limits of usefulness, (2) their sensitivity as a function of acceleration level, threshold and magnitude of zero shift, and (3) the change in basic sensitivity due to high shock loads.

* This "guess" is based on analysis of a versed sine pulse.

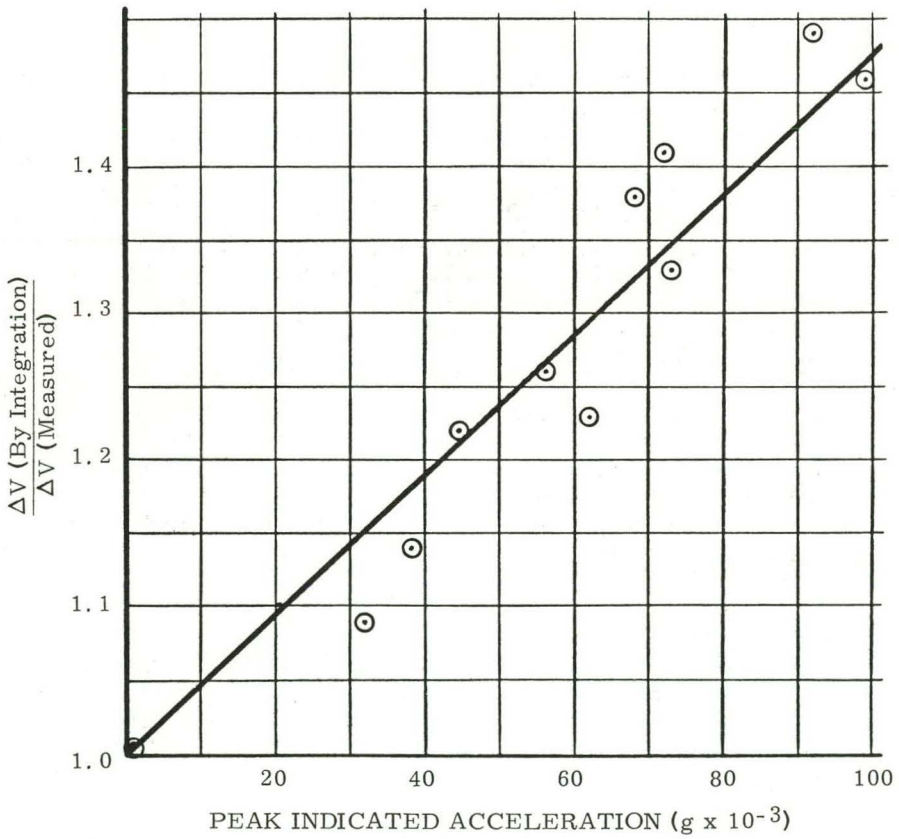

Figure 13 - Plot of ratio of velocity change obtained by integrating the acceleration-time trace to actual measured velocity change versus indicated peak acceleration. Area and peak both based on the accelerometer low-level sensitivity.

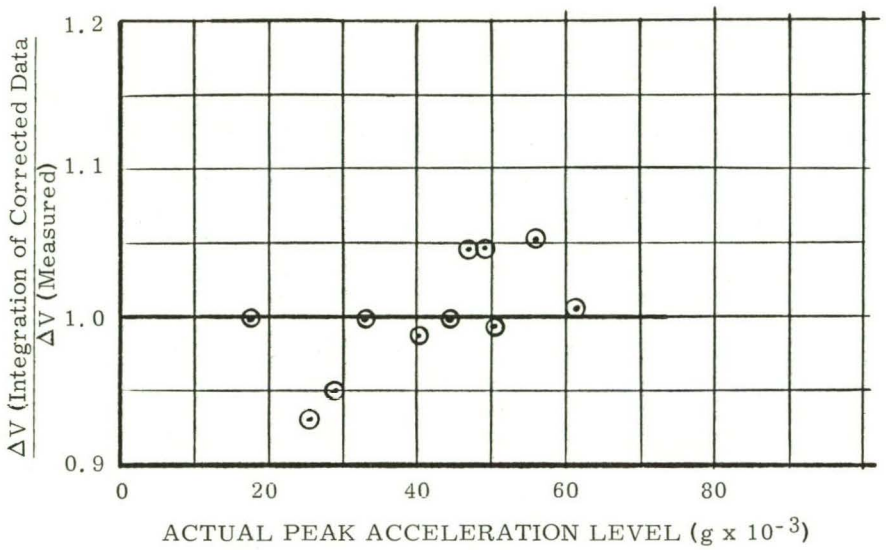

Figure 14 - Plot of ratio of velocity change obtained by integrating the acceleration-time trace versus measured velocity change. Area and peak acceleration both corrected for linear change in accelerometer sensitivity, assuming the accelerometer sensitivity to have increased by 100 percent at 100,000 g

APPENDIX

The relatively high velocity changes (i. e., > 200 fps) required for the 100,000 g shock pulses suggested a small air gun as a velocity generator. For ease in operation it was desirable to obtain a gun that would require neither a seal nor mechanical restraint on the projectile to be fired. The operation of our pneumatic actuators led to consideration of a kickback piston firing valve arrangement. Figure 15 is a schematic showing the features of the gun finally designed. The fire air reservoir is made from stock 1/8 OD by 1/2-inch wall seamless steel tubing. The barrel also is made from seamless steel tubing of the necessary ID to provide the desired clearance (usually about 0.020 to 0.030 inch) for the projectile. It is attached to the front plate of the gun with a quick disconnect fitting. The barrel diameters can vary within rather wide limits. This is considered a most important feature, since at Sandia we know of no other air gun where the barrel diameter can be varied easily to accommodate different test specimens. In most air guns, pistons or sabots must be built to compensate for the differences in diameter between desired projectiles and the gun barrel. In high-velocity launches, separating these sabots from a projectile in the time interval between launch and impact is often difficult.

With the reservoir charged to the firing pressure, and the projectile seated, the gun is fired by introducing trigger air against the kickback cylinder. When the trigger air is applied, the kickback piston is retracted until it is stopped by the increased set pressure. The high-pressure fire air then rushes through the slots in the kickback cylinder and acts against the projectile in the gun barrel, accelerating it forward and out of the gun. Figure 16 illustrates the firing sequence. An exploded view of the air gun is shown in Figure 17.

The outstanding features of this air gun are that it is built from standard stock tubing at a cost of about $800; neither a seal nor a mechanical release is required on the projectile; and the trigger air holds the kickback piston in the retracted position, ensuring complete removal of compressed air from the fire chamber. Also, when the trigger air is released, the kickback piston is automatically reset by the set pressure, and the gun is ready for the next test. One other important feature of this air gun is that the separation of the kickback assembly from the gun barrel permits use of a variety of barrel diameters with the one air gun.

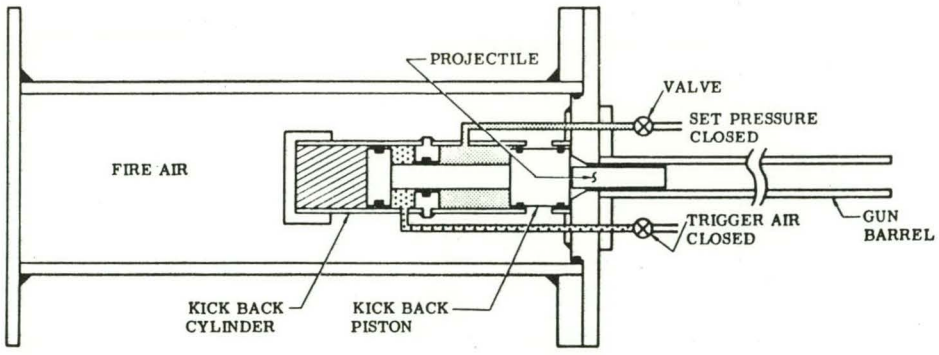

Figure 15 - Cross-section veiw of air gun

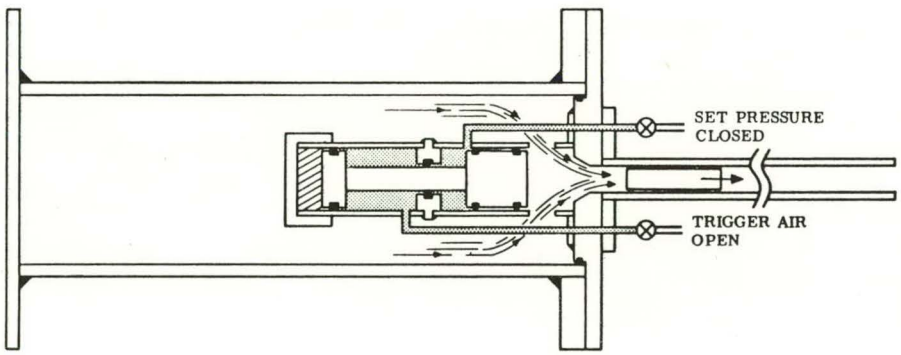

Figure 16 - Launch sequence of air gun

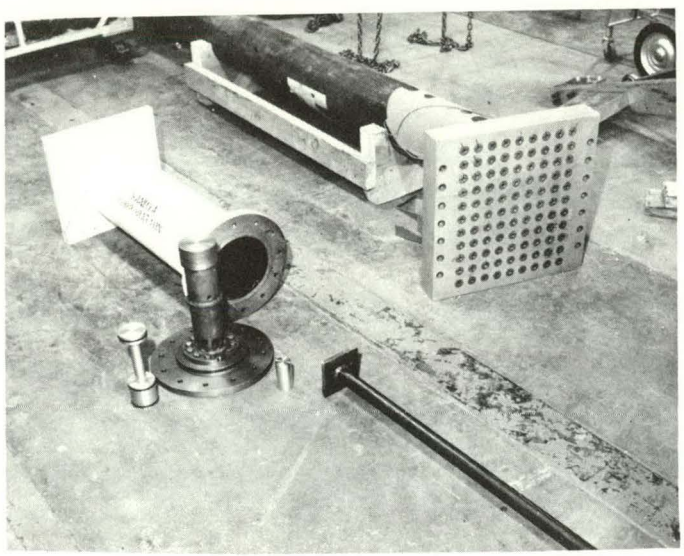

Figure 17 - Exploded view of air gun